A Machine Learning Approach to Passive Human Motion Detection Using WiFi Measurements From Commodity IoT Devices

Anisha Natarajan, Vijayakumar Krishnasamy, and Munesh Singh

***Abstract*— Human motion is a primary indicator of indoor occupancy and activity. Motion sensing has paramount importance in the energy management of modern smart buildings and is used for automated controls of lighting and heating, ventilation, and air conditioning (HVAC) equipment. The all-pervasive WiFi infrastructure in urban buildings offers an opportunistic method of human motion detection through passive sensing of WiFi received signal strength indicator (RSSI) and channel state information (CSI). This technique unfolds a plethora of building IoT-related services, in addition to sustainable energy utilization and reduced emission of greenhouse gases. In this article, a device-free human motion detection method through WiFi RSSI and CSI collected from commercial-off-the-shelf (COTS) IoT devices is proposed. Using a laptop, a smartphone, and an ESP32 as receivers, WiFi RSSI and CSI samples were collected from two residential buildings, to constitute six datasets. A 4-D feature vector that exploits the data spread in the time domain is extracted from the collected samples and used to train a two-stage ensemble machine learning model. A comparison of various RSSI-based datasets indicates a mean cross validation accuracy of up to 99.7% and 97.8% in line-of-sight (LoS) and through-the-wall scenarios, respectively. The detection accuracy in non-LoS environments can be enhanced using CSI-based features, enabling motion detection in different rooms using a single WiFi router.**

***Index Terms*— Channel state information (CSI), commodity Internet of Things (IoT) devices, ensemble learning, human motion, received signal strength indicator (RSSI).**

I. Introduction

INTERNET of Things (IoT) for smart buildings is a holistic framework for intelligent utilization of building resources, to enhance the energy-efficient behavior, safety, and comfort of its occupants. Rapid increase in building floor area and rising energy requirements for lighting, space heating/cooling, and plug loads have made buildings a major source of energy-related greenhouse gas emissions [1]. Real-time monitoring of occupant's energy demand through data-driven analysis of a variety of sensors plays a vital role in minimizing energy wastage and smart scheduling of loads [2]. Human motion detection is a key indicator of building occupancy and is widely deployed in urban buildings for appliance control, especially in lighting. Such sensing is primarily dominated by motion sensors that detect the intensity of infrared radiations emitted by human body [3]. The false negative rate of such passive infrared (PIR) sensors is high in locations where the ambient temperature is very high and comparable to human body. Also, they present limited scaling to other levels of occupancy detection, such as activity recognition or localization. Vision-based techniques are also widely used for tracking human motion but predominantly applied for anomaly detection [4]. Motion can also be detected using wearable strain and inertial sensors [5].

Due to the presence of diverse indoor artifacts and changing environmental parameters such as temperature and humidity, the properties of the signal arriving at a wireless receiver are affected by multipath effects such as scattering, reflection, shadowing, and fading. Whenever a human obstructs the path of a radio signal, the altered behavior of the received signal may be studied to reveal the dynamic changes in occupant behavior. Modern smart buildings, including residential spaces, are equipped with a variety of IoT-enabled devices such as WiFi routers, laptops, and smartphones. The enormous amount of WiFi traffic produced by this sensor network can be intelligently used for low-cost and noninvasive human motion detection. Although the characteristics of the WiFi signals are dependent on environmental conditions and layout of the indoor environment, they can offer coverage even behind walls, contrary to the existing PIR and camera-based detection techniques. Unlike vision-based techniques using various types of cameras, WiFi-based passive occupant sensing preserves user privacy—a key factor in residential buildings, while enabling accurate detection. Received signal strength indicator (RSSI) and channel state information (CSI) are two vital parameters of a WiFi signal that reflect the changes in the signal propagating environment [6], [7]. While all commodity IoT devices can report RSSI, physical layer channel information or CSI can be reported only on specialized hardware [8], [9], [10], [11], [12]. These devices require firmware modifications to report CSI and have limited adoption in low-cost and portable IoT-based applications. In this work, we have proposed a simple and low-complexity

Manuscript received 14 December 2022; revised 10 April 2023; accepted 12 April 2023. Date of publication 10 May 2023; date of current version 15 May 2023. This work was supported by the Visvesvaraya Ph.D. Scheme, Ministry of Electronics and Information Technology, Government of India. The Associate Editor coordinating the review process was Dr. Huang-Chen Lee. *(Corresponding author: Vijayakumar Krishnasamy.)*

Anisha Natarajan and Vijayakumar Krishnasamy are with the Department of Electronics and Communication Engineering, Indian Institute of Information Technology, Design and Manufacturing Kancheepuram, Chennai 600127, India (e-mail: edm20d001@iiitdm.ac.in; vijayakumar@iiitdm.ac.in).

Munesh Singh is with the Department of Computer Science and Engineering, Indian Institute of Information Technology Design & Manufacturing Jabalpur, Dumna 482005, India (e-mail: munesh.singh@iiitdmj.ac.in).

Digital Object Identifier 10.1109/TIM.2023.3272374

device-free human motion detection model that exploits WiFi RSSI and CSI extracted from three unmodified commodity IoT devices including a laptop, a smartphone, and an ESP32. In our study, we have used WiFi samples collected from a single transmitter–receiver antenna pair, to accurately detect human motion in line-of-sight (LoS) and through-the-wall conditions. The major contributions of this work are given below.

1) This work proposes an accurate and low-complexity model, for human motion detection in an indoor environment, which leverages single-link RSSI and CSI measurements collected from commodity IoT devices.
2) It proposes a unique feature set based on the time-domain spread-based features of WiFi samples for classifying human motion using ensemble learning models, in LoS and through-the-wall scenarios.
3) It validates model performance by investigating different walk directions and speeds, multiple occupant scenarios, and effect of static activities.

The structure of this article is as follows. Section II gives a primer on human motion detection using WiFi RSSI and CSI. A detailed description of the proposed model and the experimental setup are presented in Sections III and IV, respectively. Section V provides a discussion of the results, followed by concluding remarks and future directions in Section VI.

II. WiFi-Based Human Motion Detection for Energy Saving in Smart Buildings

Fig. 1 presents the overview of an occupancy-driven load control model for smart buildings, based on the human motion detection model proposed in this article. In this approach, IoT devices such as ESP32 may be used to collect WiFi frames transmitted from commercial-off-the-shelf (COTS) WiFi routers that are already available in the building for Internet connectivity. The acquired samples are transferred to the proposed human motion detection model, described in Section III, for online occupancy prediction. Such real-time predictions may be used to trigger the on/off controls of lighting and heating, ventilation, and air conditioning (HVAC) loads through smart switches or through the combination of an ESP32 with a relay. As envisaged in this article and elaborated in Sections II–V, the ESP32 could be replaced by commercial WiFi receivers such as laptops or smartphones. The proposed machine learning model can be run on a local server or a cloud-based database for online motion prediction. Alternatively, the trained model could also be deployed on edge devices, for enhanced response time and data security.

The IoT devices used in this study are powered using rechargeable batteries, and their recharge interval is a significant parameter deciding the energy efficiency of the system. Suppose the ESP32 is used as a stand-alone device for walk detection and is powered using a 3.2-V, 6000-mAh lithium iron phosphate rechargeable battery. The current drawn by ESP32 in active power mode with WiFi in listening mode is ≈100 mA [13]. Assuming that the motion sensing system is operated 10 h a day, the battery drain per day is 1000 mAh and the battery recharge interval is ≈6 days.

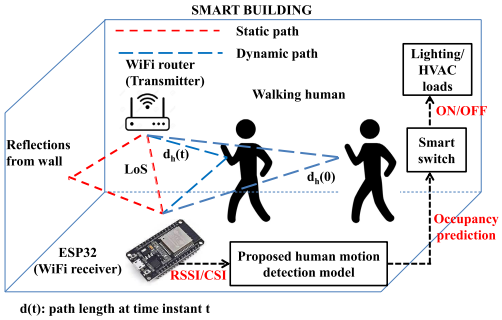

Fig. 1. Indoor multipath signal propagation scenario in a smart building with occupant-centric load control.

The proposed approach uses WiFi samples from laptops and smartphones and hence offers an opportunistic method of motion sensing with zero capital cost. In the case of ESP32, the device and battery costs constitute the overall system cost. ESP32 chips are available at a price of U.S. 4$ with various development boards having prices ranging up to U.S. 8$. Combining the battery cost of U.S. 4$, the capital cost of such a system is only U.S. 12$. Although PIR-based motion sensors are available at <1$, they are non-IP devices and need to be connected to another IP-based device to invoke any IoT-based application, making the overall cost comparable to the proposed ESP32 based motion detection system. Hence, the proposed model offers an accurate and cost-effective IoT-driven solution for human motion sensing and can be considered as an easy replacement for the existing PIR motion sensors.

A. Effect of Human Behavior on WiFi RSSI and CSI

The signal arriving at a wireless receiver is affected by diverse artifacts present in the propagation environment. As shown in Fig. 1, the transmitted signal suffers multiple reflections, scattering, and fading during its travel from the transmitter to the receiver and hence contains useful information about the environment dynamics [14]. WiFi RSSI and CSI are two important signal metrics that may be used to study the changes in the indoor propagation environment, such as human motion.

RSSI in dBm is related to the distance d between the transmitter and the receiver by

$$\text{RSSI} = -(10n\log(d) + A). \tag{1}$$

Here, n is the path loss exponent (1.5-5 in an indoor environment). A is the RSSI in dBm at 1-m distance from the WiFi transmitter. Fig. 2(a) depicts the average RSSI measurements at varying distances from a WiFi router placed in room A of house-2, as described in Section IV. By fitting a curve through these measured values, the estimated value of indoor path loss exponent is 2.741, within 95% confidence bounds. Although RSSI gives a coarse representation of the propagation channel, Fig. 2(c) shows the large-amplitude fluctuations in RSSI values when a moving human is present in the environment, compared with measurements in a vacant room [Fig. 2(b)]. Any COTS IoT device can report RSSI values.

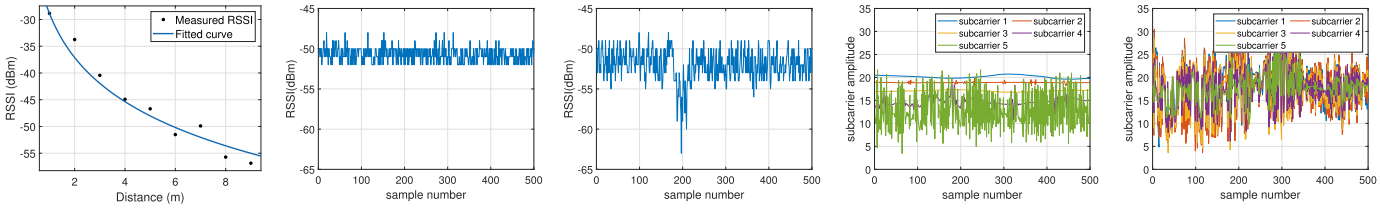

Fig. 2. WiFi RSSI and CSI (a) variation in WiFi RSSI with distance. (b) RSSI in a vacant room. (c) RSSI with walking user. (d) CSI in a vacant room. (e) CSI with walking user.

CSI is a matrix of complex values, representing the amplitude and phase of WiFi orthogonal frequency division multiplexing (OFDM) subcarriers and contains detailed information about the channel dynamics. For the multipath signal propagation scenario depicted in Fig. 1, the channel frequency response (CFR) $H(f,t)$ may be represented as

$$H(f,t) = a_{\text{LOS}}(f)e^{-j2\pi f \tau_{\text{LOS}}} + a_{\text{ref}}(f)e^{-j2\pi f \tau_{\text{ref}}} + a_h(f,t)e^{-j2\pi f \tau_h(t)}. \quad (2)$$

Here, $a_{\text{LOS}}(f)$, $a_{\text{ref}}(f)$, and a_h represent the attenuation coefficients of the LoS path, reflections from walls and ceiling, and from walking human, respectively. $\tau_{(.)}$ is the delay of the corresponding path. The first two terms in the above equation may be combined together to represent the response of the static paths and is rewritten as $H_s(f) = a_s(f)e^{-j\phi_s}$

$$H(f,t) = H_s(f) + a_h(f,t)e^{-j2\pi \frac{d_h(t)}{\lambda}}. \quad (3)$$

Here, $d_h(t)$ is the distance moved by the human at the tth instant and λ is the signal wavelength. $|H(f,t)|^2$ is the CFR power, given by

$$\begin{aligned} \left|H(f,t)\right|^2 &= H(f,t)H^*(f,t) \\ &= \left|a_s(f)\right|^2 + a_h(f,t)a_s^*(f)e^{\phi_s - j2\pi \frac{d_h(t)}{\lambda}} \\ &\quad + a_h^*(f,t)a_s(f)e^{j2\pi \frac{d_h(t)}{\lambda} - \phi_s} + \left|a_h(f,t)\right|^2 \\ \left|H(f,t)\right|^2 &= \left|a_s(f)\right|^2 + \left|a_h(f,t)\right|^2 \\ &\quad + 2\left|a_h(f,t)a_s(f)\right| \cos\left(2\pi \frac{d_h(t)}{\lambda} - \phi_s\right). \end{aligned} \quad (4)$$

Assuming that the human is moving with a uniform velocity v, $d_h(t)$ can be rewritten as

$$d_h(t) = d_h(0) + vt. \quad (5)$$

Then

$$\left|H(f,t)\right|^2 = \left|H_s(f)\right|^2 + \left|a_h(f,t)\right|^2 + 2\left|a_h(f,t)H_s(f)\right| \cos\left(2\pi \frac{d_h(0) + vt}{\lambda} - \phi_s\right). \quad (6)$$

An examination of the third term in the above expression suggests that the presence of a human obstacle and his/her velocity of motion can substantially affect the channel response. The CFR in an IEEE 802.11 OFDM system is reported as CSI. The CSI of the kth subcarrier, for the ith transmitting antenna and jth receiving antenna, is given as

$$H_k(i,j) = \left|H_k(i,j)\right|e^{j\theta_k(i,j)}. \quad (7)$$

A limited set of hardware devices have the capability to report CSI, restricting the usage of CSI-based sensing in commercial applications. This includes WiFi chipsets such as Intel WiFi Link 5300 [8], Qualcomm Atheros [9], Broadcom and Cypress chipsets in Raspberry Pi 3B+ and certain smartphones [10], and ESP32 [11], [12]. The ESP32 microcontroller can report RSSI and CSI values without any firmware changes and hence used in the proposed work. Fig. 2(d) shows the amplitude of the first five OFDM subcarriers in an empty room. The first four subcarriers exhibit minimum noise, while subcarrier 5 is uncorrelated and noisy. It can be observed that in Fig. 2(e), all the subcarriers have large fluctuations across the mean amplitude and exhibit correlated variations in the presence of human motion [14].

B. Related Work

WiFi RSSI and CSI can be used to detect human motion through diverse techniques such as thresholding, mathematical modeling, machine learning, or deep learning. A summary of the related work is given in Table I. Booranawong et al. [15] have developed a system to sense and track human motion in three different zones by thresholding of WiFi RSSI. After denoising the samples using a weighted average filter, the RSSI thresholds for human presence in each zone were determined by studying the deviation of the samples from the mean value, when the respective zone was vacant. Different movement patterns and walking speeds were explored in this study. The authors have also proposed an adaptive RSSI filtering scheme, which also filters only those samples whose variation levels are greater than two times the standard deviation, hence reducing the computational complexity [16]. Probabilistic modeling of human motion through RSSI measurements is another approach to characterize the effect of human presence on the LoS path [17].

Qian et al. [18] have classified human motion in LoS environments using features based on maximum eigenvalues of CSI amplitude and phase covariance matrices. Wu et al. [19] have used the eigenvalues of CSI amplitude and phase matrices to classify human motion. This is based on the observation that normalized eigenvalues lie close to 1 in the absence of human motion and fall significantly in the presence of moving targets. By estimating the phase difference of CSI subcarriers in a two-antenna system, Gu et al. [20] have proposed a motion detection system that accurately distinguishes mobile states from stationary states. Stationary states are estimated using thresholding, and noisy subcarriers are eliminated by Euclidean distance computation. In [21] and [22], the authors

TABLE I
SUMMARY OF RELATED WORK

Reference	Signal	Receiver	Denoising	Through-the-wall	Human Behaviour	Methodology
[15],[16]	RSSI	CC2500 RF transceiver	Weighted moving average filter	No	Walking- different speeds and directions, multiple people	Estimation of motion detection thresholds based on mean and standard deviation values.
[17]	RSSI	ar5006x	No	No	Walking, count	Mathematical modelling of the probability distribution of RSSI values.
[18]	CSI amplitude and phase	Intel 5300	Hampel filter	No	Walking-different speeds, stationary	Classification using eigen value of covariance matrix
[19]	CSI amplitude and phase	Intel 5300	Hampel filter	No	Walking, sitting and standing	Walk detection by estimating maximum eigenvalues of CSI correlation matrix.
[20]	CSI phase	Intel 5300	Butterworth filter	No	Walking, standing up, sitting down, falling	Subcarrier selection by computing Euclidean distance, motion detection by thresholding of derivative of CSI phase difference
[21]	CFR power	Intel Galileo Gen2	-	Yes	Walking, different trajectories	Statistical modeling based on autocorrelation function of CFR power, hypothesis testing
[22]	CFR power	Intel 5300	Mean based abnormal trend elimination	Yes	Walking, different trajectories	Modeling based on distribution difference of autocorrelation sequences of CFR power
Proposed work	RSSI, CSI amplitude	Off-the-shelf laptop, smartphone & ESP32	Wavelet filter for CSI	Yes	Walking- different speeds and directions, multiple people, static (lying, sitting, standing)	Feature based ensemble machine learning model training.

have performed motion detection in LoS and through-the-wall conditions by statistical modeling of the autocorrelation sequences of CFR power.

It may be observed from Table I that previous works use specialized hardware and CSI data from multiple transmitter–receiver pairs for motion detection. This increases the computational complexity of the system and hinders adoption in commercial applications. In this work, we use CSI samples from a single transmission link, collected from a low-cost IoT device, to substantially reduce the model complexity. We also demonstrate motion detection using RSSI samples collected from COTS devices such as laptops and smartphones, to further enhance the adoption rate of the proposed method. In contrast to previous works reported in [15] and [16], we use raw RSSI signals for feature extraction, to significantly reduce the preprocessing time. Unlike many previous works, we investigate the model performance on various use cases including through-the-wall conditions and multiple occupant scenarios, for both the RSSI and CSI signals.

III. PROPOSED HUMAN MOTION DETECTION MODEL

A. System Overview

An overview of the proposed motion detection system is shown in Fig. 3.

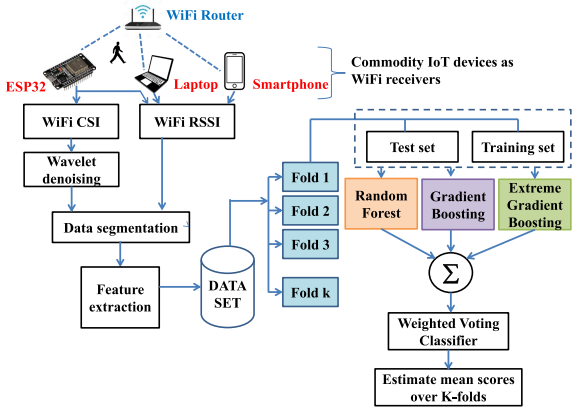

Fig. 3. System overview.

1) *Data Acquisition*: RSSI samples are collected from three commodity IoT devices, namely, a laptop, smartphone, and an ESP32 node MCU and stored as .pcap or .csv files in the host system. Samples collected from ESP32 also include the CSI values of 64 OFDM subcarriers, in addition to the RSSI value of each frame.
2) *Data Preprocessing*: The collected CSI samples are preprocessed by removing the dc component, erroneous second subcarrier, and 11 null subcarriers, to obtain 51 useful OFDM subcarriers. The CSI amplitude signals are embedded in various impulse and burst noises [23]. The performance of various smoothing and low-pass filters is studied, and a comparison is depicted in Fig. 4. To recover useful information from the CSI samples, it is necessary to retain the high-frequency variations due to human motion, while rejecting the noise due to the environment. This can be effectively done by wavelet denoising [24], [25]. In this article, Daubechies wavelet is used for CSI amplitude denoising, and the decomposition level was empirically set to 9. Raw RSSI samples are used in feature extraction. Prior to feature engineering, the samples are divided into nonoverlapping windows of fixed size.
3) *Feature Extraction*: Four features that describe the data spread in the time domain, namely, *variance, mean absolute deviation (MAD), range*, and *inter quartile*

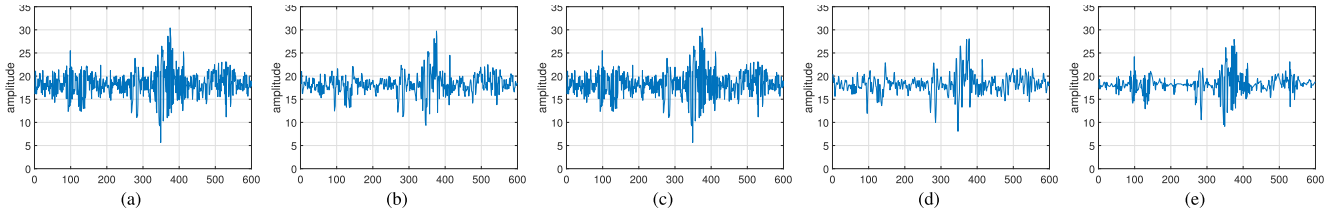

Fig. 4. WiFi CSI denoising filters. (a) Original CSI amplitude of a walking user. (b) Moving mean filter. (c) Savitzky–Golay filter. (d) Third-order Butterworth low-pass filter. (e) db4 wavelet denoising.

range (IQR), are extracted from the segmented raw RSSI and denoised CSI samples. The features are separately labeled as *empty* and *walking*, to constitute a binary classification dataset. The size of the feature matrix for the RSSI dataset is 4× the number of samples, whereas for the CSI dataset, the dimension is (the number of subcarriers ×4) × the number of samples.

B. Feature Extraction

A mathematical description of the features extracted from CSI samples is given below. Let N be the number of subcarriers, P be the number of packets, and $x_{i,k}$ be the amplitude of the kth subcarrier in the ith packet, where $k \in \{1, N\}$ and $i \in \{1, P\}$. For a window of size w packets ($w < P$), a window of CSI amplitudes can be represented as

$$\mathbf{W}_{w\times N} = \begin{bmatrix} x_{1,1} & x_{1,2} & \cdots & x_{1,N} \\ x_{2,1} & x_{2,2} & \cdots & x_{2,N} \\ \vdots & \vdots & \ddots & \vdots \\ x_{w,2} & x_{w,2} & \cdots & x_{w,N} \end{bmatrix}. \tag{8}$$

The mean amplitude of the kth subcarrier is

$$\mu_{s_k} = \frac{\sum_{j=1}^{w} x_{j,k}}{w}; \quad k \in \{1, N\}. \tag{9}$$

Then, the variance is given by

$$\text{var}_{s_k} = \sum_{j=1}^{w} \left(x_{j,k} - \mu_{s_k}\right)^2. \tag{10}$$

MAD of the kth subcarrier may be computed as

$$\text{mad}_{s_k} = \frac{1}{w} \sum_{j=1}^{w} \left|x_{j,k} - \mu_{s_k}\right|. \tag{11}$$

The range of each subcarrier in a window W can be represented as

$$\text{range}_{s_k} = \max\left(x_{j,k}\right) - \min\left(x_{j,k}\right); \quad k \in \{1, N\}, \ \ j \in \{1, w\}. \tag{12}$$

Similarly, the IQR is given by

$$\text{iqr}_{s_k} = 75^{th} \text{ Percentile}\left(x_{j,k}\right) - 25^{th} \text{ Percentile}\left(x_{j,k}\right). \tag{13}$$

Computing the features from all N subcarriers constitutes a row vector

$$\text{Feature}(\mathbf{W}) = \begin{bmatrix} f_{s_1} & f_{s_2} & \cdots & f_{s_{N-1}} & f_{s_N} \end{bmatrix} \tag{14}$$

where f denotes the above-mentioned feature set. In case of RSSI samples, the window matrix $\mathbf{W}$ is replaced by a column vector of RSSI values.

C. Proposed Ensemble Learning Model

Ensemble learning is a powerful and efficient machine learning approach that can produce robust and accurate classification results, by aggregating the outputs of several base learners. A two-stage ensemble machine learning model is proposed in this article to classify human motion. Stage-1 consists of the following tree-based ensemble machine learning classifiers.

1) *Random Forest*: In this model, weak decision trees are fit on subsamples of the original dataset and the ensuing results are averaged out. This method is also called bootstrap aggregation or bagging and may be used to produce more accurate classification results than a single decision tree.
2) *Gradient Boosting*: It is a sequential model, where each subsequent model corrects the error of the prior model by giving higher weights to misclassified data points.
3) *Extreme Gradient Boosting (XG Boost)*: It is an improved version of the gradient boosting (GB) machine and uses a parallel implementation for reducing the processing time.

Stage-2 uses a *weighted voting classifier* as the meta-learner and combines the predictions from the above-mentioned base learners. The weights for each base learner are determined empirically, giving higher weight to the base model that produces more accurate classification results. Both *hard* and *soft voting* classifiers are examined in the proposed model.

IV. Experiment Setup

WiFi data were collected from two houses at varying data sampling rates for both the LoS and non-LoS conditions. The layout of the houses is shown in Fig. 5. Commercial WiFi routers already available in the house for Internet connectivity and operating at 2.4-GHz center frequency and 20-MHz bandwidth were used as transmitters. A Lenovo laptop with a Windows application installed on it, a Redmi 8A smartphone with an Android app [26], and an ESP32 MCU were used as WiFi receivers. The laptop and smartphone are able to collect RSSI samples, while ESP32 can report both RSSI and CSI [11], [12]. The application installed on the laptop collects samples at 5-s intervals. For the smartphone and ESP32-based data collection, sampling was performed at a higher rate. This is achieved by sending a flood of Internet Control Message Protocol (ICMP) sequences to the router and collecting the RSSI and CSI values of the corresponding responses. For datasets 2–6, the sampling rate was between 80 and 100 Hz. The laptop and smartphone are configured as active clients to the WiFi router, while the ESP32 was

TABLE II
DATASET SUMMARY

Parameter	Dataset 1	Dataset 2	Dataset 3	Dataset 4	Dataset 5	Dataset 6
Location	H-1	H-2, R-A	H-2, R-A	H-2, R-A	H-2, R-B	H-2, R-C
Sampling rate	0.2 Hz	80Hz	80 Hz	100 Hz	80 Hz	80 Hz
Feature window size	10 min	6 s	6 s	6 s	6 s	6 s
WiFi Router	ZTE	Alphion	TP-Link	Alphion	Alphion	Alphion
Receiver	Laptop	Smartphone	ESP32	ESP32	ESP32	ESP32
WiFi Metric	RSSI	RSSI	RSSI	RSSI	RSSI&CSI	RSSI&CSI
Location of Tx and Rx	LoS	LoS	LoS	LoS	non LoS	non LoS
No. of participants	3	1	2	2	1	2
No. of samples	100	411	530	581	481	565

Tx: Transmitter, Rx: Receiver, H:House, R: Room

TABLE III
COMPARISON OF MEAN CROSS VALIDATION SCORES (IN %) FOR LOS CONDITION

Classifier	Dataset 1				Dataset 2				Dataset 3				Dataset 4			
	Acc	Prec	Rec	F1	Acc	Prec	Rec	F1	Acc	Prec	Rec	F1	Acc	Prec	Rec	F1
Random Forest	**86**	**89.2**	84	85.4	93.9	92.9	**94.5**	93.6	**99.7**	**100**	**98.8**	**99.3**	**94**	93.4	**94.7**	93.9
Gradient Boosting	83	88.7	77.8	81.1	93	92.7	92.3	92.3	99.1	98.5	**98.8**	98.6	92.5	92.4	92.8	92.4
XG Boost	**86**	85.6	**88.5**	**85.7**	93.9	92.8	94.4	93.5	99.5	99.3	**98.8**	99	93.8	93.2	94.8	93.9
Hard Voting	**86**	**89.2**	84	85.4	93.9	92.9	**94.5**	93.6	99.5	99.3	**98.8**	99	93.6	93.2	94.3	**94**
Soft Voting	85	88.7	82	84.1	**94.2**	**93.3**	**94.5**	**93.7**	99.3	98.9	**98.8**	98.8	**94**	**94**	94.3	**94**

Acc:Accuracy, Prec:Precision, Rec: Recall, F1-F1 score

TP: True Positive, TN: True Negative, FP: False Positive, FN: False Negative

$$Accuracy = \frac{TP+TN}{TP+FP+TN+FN}, Precision = \frac{TP}{TP+FP}, Recall = \frac{TP}{TP+FN}, F1 = \frac{2\times(Precision)\times(Recall)}{Precision+Recall}$$

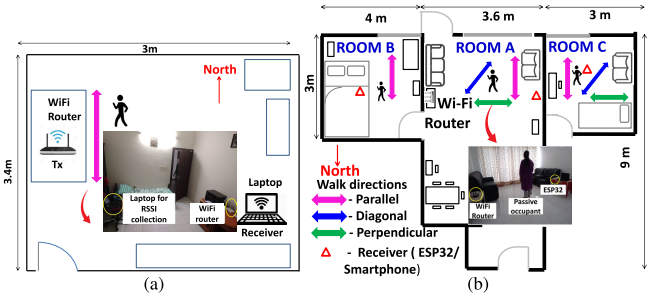

Fig. 5. Layout of the experimental site. (a) House 1. (b) House 2.

configured in promiscuous mode so as to sniff the WiFi frames of the configured channel frequency.

Dataset 1 was constructed using samples from house 1, while datasets 2–6 were collected from three different rooms in house 2. Data were collected from the sites during vacant condition and when the participants were walking. Features were extracted from these samples and were annotated as class 0 (empty) and class 1 (moving), respectively. A summary of the datasets is given in Table II.

V. RESULTS AND DISCUSSION

All the models were subject to tenfold cross validation, and their mean scores are compared for various performance metrics, namely, accuracy, precision, recall, and F1 score. The model accuracy on unseen data using test–train split method was also studied. The memory footprint of the trained models, their training, and prediction time were also analyzed.

A. LoS Condition

The mean prediction scores for datasets 1–4, where the transmitter and receiver are located in LoS condition, are depicted in Table III and the corresponding model parameters in Table IV. Owing to low rate of sample collection from the laptop, the mean prediction accuracy of dataset 1 is only 86%, while it exhibits a reasonably good precision of 89.2%. A major share of the room area is occupied by various kinds of furniture, and the increased scattering and reflections from these also account for the reduced accuracy. Random forest (RF) and hard voting classifiers perform well on this dataset and give comparable prediction scores. Features extracted from dataset 2 have a good degree of classification ability and perform well on all the metrics. Among all the classifiers, soft voting attains the best scores for all the parameters. This shows that smartphone RSSI may be opportunistically used for motion detection, to invoke a host of IoT-enabled services.

Datasets 3 and 4, constituted using RSSI collected from ESP32, reveal a high degree of prediction scores, with the best results manifested by dataset 3, using the RF classifier. The slightly lower scores on dataset 4 may be attributed to the higher noise level in the RSSI samples, as they are collected at 100-Hz rate and also due to the heterogeneity in user motion. Soft voting classifier offers equivalent performance as that of RF classifier, on the aforementioned datasets.

B. Non-LoS Condition

Datasets 5 and 6 are constructed using WiFi samples collected in an NLoS situation, with the WiFi router and receiver ESP32 placed in different rooms. For dataset 5, the samples were collected in a complete NLoS situation, with the doors and windows of the room kept closed. On the contrary, in dataset 6 a partial NLoS set up was used and the door was left open during sample collection. Tables V and VI depict the mean cross validation scores of all the classifiers and the corresponding model parameters, respectively.

TABLE IV
COMPARISON OF MODEL PARAMETERS FOR LOS CONDITION

Classifier	Trees	Depth	Dataset 1			Dataset 2			Dataset 3			Dataset 4		
			Mem	TT	PT	Mem	TT	PT	Mem	TT	PT	Mem	TT	PT
Random Forest	50	37	92	166.5	1.8	87	265.23	17.65	54	118.2	5.1	194	112	5.4
Gradient Boosting	50	20	147	103.7	**0**	161	**224.54**	**4.84**	134	102.3	**3.5**	322	**209.5**	**4.8**
XG Boost	50	20	**47**	**61.6**	7	**51**	229.81	6.76	**35**	**86.3**	6.4	**81**	272.5	**4.8**
Hard Voting	-	-	286	234.2	15.6	298	686.23	71.19	221	312.4	31.2	596	328	15.6
Soft Voting	-	-	286	968.5	62.4	298	328.16	51.17	221	562.3	78.1	596	374.8	15.6

Mem: Memory (KB), TT: Training Time(ms), PT: Prediction Time (ms)

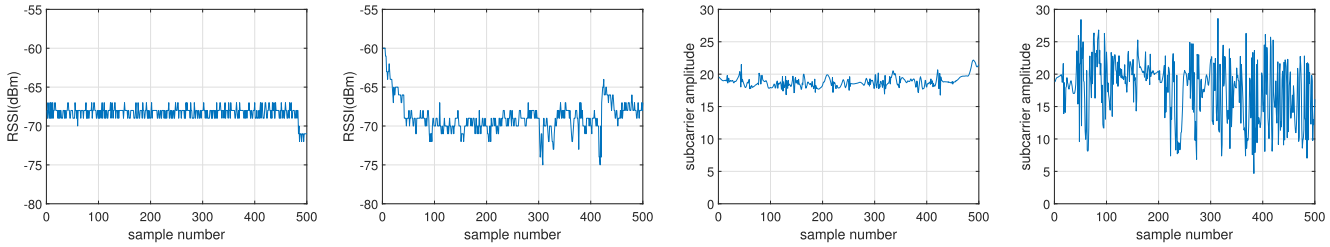

(a) (b) (c) (d)

Fig. 6. WiFi RSSI and CSI in NLoS conditions. (a) RSSI in vacant room. (b) RSSI with walking user. (c) CSI in vacant room. (d) CSI with walking user.

TABLE V
COMPARISON OF MEAN CROSS VALIDATION SCORES (IN %) FOR NLOS CONDITION

Classifier	Dataset 5-RSSI				Dataset 5-CSI				Dataset 6-RSSI				Dataset 6-CSI			
	Acc	Prec	Rec	F1	Acc	Prec	Rec	F1	Acc	Prec	Rec	F1	Acc	Prec	Rec	F1
Random Forest	**83.4**	**78.9**	**85.3**	**81.4**	**99.8**	**99.5**	**100**	**99.8**	97.7	**98.6**	96.8	97.6	99.8	99.6	**100**	99.8
Gradient Boosting	81.1	78.2	80.3	78.4	99.6	99	**100**	99.5	97.1	98	96.6	97.2	**100**	**100**	**100**	**100**
XG Boost	81.7	78	82.7	79.7	99.6	**99.5**	99.6	99.6	97.7	**98.6**	96.9	97.7	99.8	99.6	**100**	99.8
Hard Voting	82.5	78.4	84.6	80.7	**99.8**	**99.5**	**100**	**99.8**	97.7	**98.6**	96.8	97.6	99.8	99.6	**100**	99.8
Soft Voting	82.1	78.3	83.7	80.2	**99.8**	**99.5**	**100**	**99.8**	**97.8**	**98.6**	**97.2**	**97.9**	99.8	99.6	**100**	99.8

TABLE VI
COMPARISON OF MODEL PARAMETERS IN NLOS CONDITION

Classifier	Dataset 5-RSSI			Dataset 5-CSI			Dataset 6-RSSI			Dataset 6-CSI		
	Mem	TT	PT	Mem	TT	PT	Mem	TT	PT	Mem	TT	PT
Random Forest	309	**71.3**	32.3	**28**	**284.5**	19.8	93	**67.69**	16.62	**28**	**108.47**	1.99
Gradient Boosting	464	179	**3.9**	63	1169.6	2	165	81.95	**4.87**	73	1371.71	2.29
XG Boost	**123**	229.2	16.7	31	491.7	**0**	**47**	188.39	42.37	31	263.05	**0**
Hard Voting	895	371.1	16.3	121	1506.8	33.2	131	313.18	16.69	131	1863.13	48.03
Soft Voting	895	487.1	26.3	121	1441	34.3	304	282.63	33.37	131	1684.71	37.23

Degradation of signal power reduces the performance of RSSI-based motion detection in NLoS environment, as evident in Fig. 6. It can be observed that RSSI samples exhibit comparatively lower sensitivity to human motion in NLoS environments, while signal fluctuations are much higher for the corresponding CSI samples. This leads to a lower prediction accuracy of 83.4% on RSSI samples from dataset 5. At the same time, the features extracted from the corresponding CSI samples are able to well distinguish walking humans in through-the-wall scenarios. All the models show high degree of prediction performance on this dataset, with RF and voting classifiers offering the best scores. In the case of dataset 6, although the transmitter–receiver spacing is larger than that in dataset 5, the performance of RSSI and CSI is comparable, due to the opened door. Also, datasets 5 and 6 were collected using different WiFi channels, which could be a possible cause for this disparity. The sensitivity of human motion to different WiFi channel frequencies is left for future study.

TABLE VII
MODEL ACCURACY ON UNSEEN DATA (IN %) FOR LOS CONDITION

Classifier	Dataset 1	Dataset 2	Dataset 3	Dataset 4
Random Forest	**96.66**	**95.16**	**100**	**95.59**
Gradient Boosting	93.33	93.54	**100**	92.45
XG Boost	93.33	**95.16**	**100**	94.33
Hard Voting	93.33	**95.16**	**100**	94.96
Soft Voting	93.33	94.35	**100**	93.7

C. Performance on Unseen Data

The accuracy of the trained models on an unseen test data, created by splitting the dataset into 70% training and 30% test data, is given in Tables VII and VIII for LoS and NLoS environments, respectively. All the models show accuracies >93% on all RSSI-based datasets in LoS conditions. This shows that WiFi RSSI is a worthy contender for motion detection when transmitter and receiver devices are in LoS condition.

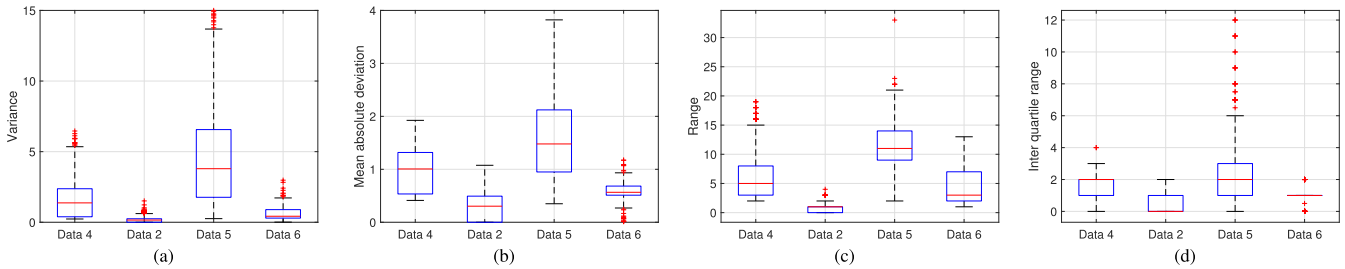

Fig. 7. Boxplot of features extracted from the RSSI dataset. (a) Variance. (b) MAD. (c) Range. (d) IQR.

TABLE VIII
MODEL ACCURACY ON UNSEEN DATA (IN %) FOR NLOS CONDITION

Classifier	Dataset 5 RSSI	Dataset 5 CSI	Dataset 6 RSSI	Dataset 6 CSI
Random Forest	**78.62**	**100**	95.2	99.4
Gradient Boosting	75.17	**100**	95.2	**100**
XG Boost	75.86	**100**	**96.4**	99.4
Hard Voting	75.86	**100**	95.2	99.4
Soft Voting	76.55	**100**	95.8	99.4

TABLE IX
CROSS-DOMAIN PERFORMANCE COMPARISON OF THE RSSI DATASETS AFTER TRAINING ON DATASET 4

Classifier	Test Dataset		
	Dataset 2	Dataset 5	Dataset 6
Random Forest	**69.35**	53.10	77.84
Gradient Boosting	**69.35**	53.79	71.85
XG Boost	**69.35**	51.72	**78.44**
Hard Voting	**69.35**	52.41	77.84
Soft Voting	**69.35**	**54.48**	77.84

As expected, motion detection accuracy falls in through-the-wall situation to as low as 75% for the RSSI-based dataset 5. But the CSI-based datasets 5 and 6 perform very well on the unseen data, irrespective of the distance from the WiFi transmitter and the presence of obstacles such as concrete walls.

The cross-domain classification ability of the models is suitable in analyzing the dependence of the trained models on the environment and the devices used for data collection. For this purpose, the model trained on dataset 4 was tested on RSSI datasets 2, 5, and 6. As indicated in Table IX, when the model trained on ESP32-RSSI in room A is tested on RSSI collected using a smartphone, the model performance needs improvement, while the maximum score obtained on the ESP32-RSSI dataset collected from room C is 78.44%. The test score drops to as low as 51.72% when tested on room B. These results can be validated by examining the boxplots of the features extracted from the aforementioned datasets, as shown in Fig. 7. The boxplots of dataset 4 show close resemblance with dataset 6 for all the four features, while a major share of the data points in dataset 5 is completely unseen by dataset 4, leading to poor testing performance. As evident from the layout of house 2, the signals arriving at room C share a common propagation environment with room A, and hence the similarity in datasets 4 and 6. Hence, the cross validation among datasets shows that to achieve the prediction accuracies mentioned in the previous sections, the model may require retraining in new environments and also when heterogeneous devices are involved in training and test data collection.

D. Model Complexity

Various model parameters, namely, the number and depth of the decision trees used in the base learners, the memory occupied by the trained model on the disk, model training and prediction times, are compared to determine their complexity. This is depicted in Tables IV and VI for LoS and NLoS conditions, respectively. The number of estimators and the tree depth for all the tree-based base learners were determined using the grid search method for dataset 3 and then used as a benchmark for comparison with other datasets. All the models require <1 MB of memory on the disk and hence suitable for remote and standalone IoT applications. XG Boost classifier requires minimum memory among most of the datasets, followed by the RF classifier. Training and prediction times for all the base learners are in the order of ten to hundred milliseconds and hence suitable for real-time applications. Voting classifiers require comparatively higher memory space, training, and prediction times due to the two-stage prediction mechanism.

E. Feature Importance

The model complexity may be reduced further using only a single feature or a combination of features for training the model. Accuracy was chosen as the performance metric, and the mean accuracy of all the models when individual features are used for training was studied. A bar chart comparing the scores of each feature for various models and datasets is shown in Fig. 8. For the RSSI-based LoS datasets 1–4, the *range* feature shows the best performance for datasets 1, 3, and 4. All the features contribute to comparable accuracies for CSI based datasets 5 and 6. Hence by eliminating redundant features, a wise combination of features may be chosen to reduce the model complexity while retaining the model performance.

F. Walk Patterns

The direction of walking during sample collection for datasets 1–6 was chosen parallel to the North–South wall of the building, in all the rooms. Different walk directions can have varying effects on the classification ability of the model. To investigate this effect, 1138 additional samples were collected using ESP32 from rooms A and C, for two other walk directions, namely, the diagonal direction (North-East to

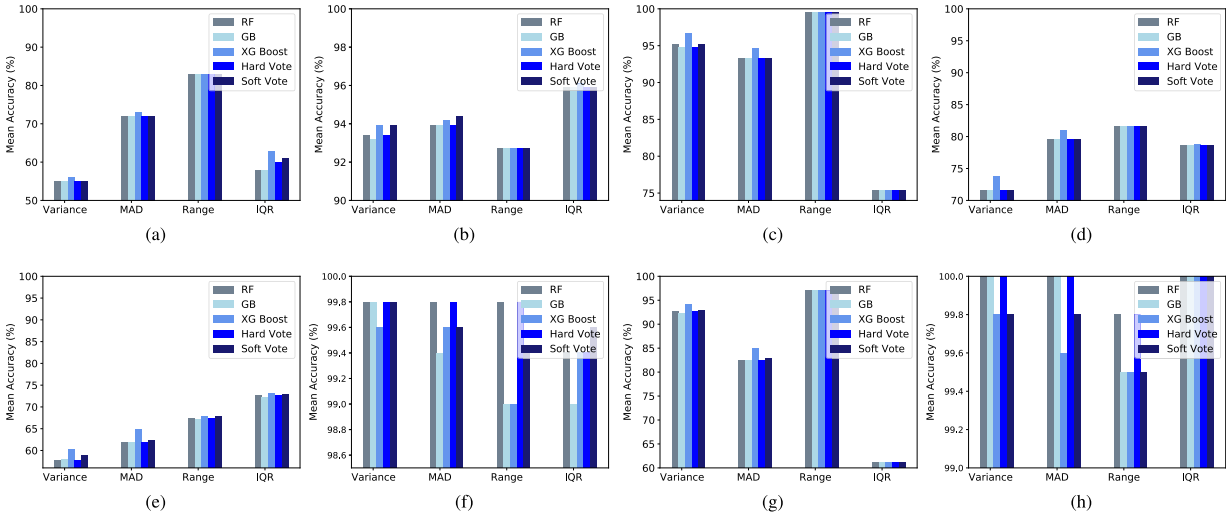

Fig. 8. Mean accuracy when individual features are used for model training. (a) Dataset 1. (b) Dataset 2. (c) Dataset 3. (d) Dataset 4. (e) Dataset 5—RSSI. (f) Dataset 5—CSI. (g) Dataset 6—RSSI. (h) Dataset 6—CSI.

TABLE X
MEAN ACCURACY (AS %) ON VARIOUS WALK DIRECTIONS—ROOM A

Classifier	Diagonal		Perpendicular	
	RSSI	CSI	RSSI	CSI
Random Forest	**100**	**100**	99.4	**99.7**
Gradient Boosting	**100**	**100**	**99.7**	**99.7**
XG Boost	**100**	99.7	**99.7**	99.4
Hard Voting	**100**	**100**	99.4	**99.7**
Soft Voting	**100**	99.7	99.4	**99.7**

TABLE XI
MEAN ACCURACY (AS %) ON VARIOUS WALK PATTERNS—ROOM C

Classifier	Diagonal		Perpendicular		Multi user	
	RSSI	CSI	RSSI	CSI	RSSI	CSI
Random Forest	72	**99.5**	73.4	**99.8**	**76.6**	**100**
Gradient Boosting	68.2	97.7	71.8	97.9	68.9	**100**
XG Boost	70.5	98.6	73.7	98.6	74.6	**100**
Hard Voting	72	**99.5**	73.4	**99.8**	**76.6**	**100**
Soft Voting	**72.3**	99.1	**75.1**	99.3	76	**100**

TABLE XII
MEAN ACCURACY (AS %) ON VARIOUS WALK SPEEDS—ROOM A

Classifier	0.57 m/s		1.19 m/s	
	RSSI	CSI	RSSI	CSI
Random Forest	**100**	**100**	**99.4**	99.7
Gradient Boosting	**100**	**100**	**99.4**	**100**
XG Boost	**100**	99.4	**99.4**	99.4
Hard Voting	**100**	**100**	**99.4**	99.7
Soft Voting	**100**	99.7	**99.4**	99.4

TABLE XIII
MEAN ACCURACY (AS %) ON VARIOUS WALK SPEEDS—ROOM C

Classifier	0.57 m/s		1.19 m/s	
	RSSI	CSI	RSSI	CSI
Random Forest	**95.2**	**99.8**	99.4	**100**
Gradient Boosting	94	**99.8**	**99.6**	**100**
XG Boost	94.6	99.6	99.4	99.6
Hard Voting	**95.2**	**99.8**	99.4	**100**
Soft Voting	95	99.6	99.4	99.8

South-West corner) and a direction perpendicular to the North–South wall, as indicated in Fig. 5(b). The results of the cross validation scores are given in Tables X and XI. The classification results in room C indicate that motion detection using RSSI-based features is comparatively difficult in NLoS conditions, for diagonal and perpendicular walk directions. The best scores in the aforementioned use cases are provided by the Soft Voting classifier, but the accuracies fall by at least 22.7% compared with the prediction scores shown in Table V.

The average walking speed of the participants during sample collection for datasets 1–6 was 0.88 m/s. The effect of varying the walk speed was studied by collecting samples at two other average walk speeds, namely, 0.57 and 1.19 m/s. For this purpose, 1262 samples were collected from rooms A and C with a parallel walk direction, and the corresponding mean accuracies are reported in Tables XII and XIII. Comparing the maximum accuracies for the RSSI-based feature datasets in Tables V and XIII for room C, it can be observed that for a low average speed of 0.57 m/s, the accuracy falls by only 2.6%. When the walk speed rises to 1.19 m/s, the maximum detection accuracy elevates to 99.4 %, even in NLoS scenarios. In the LoS condition, high prediction scores are obtained on all walk directions and speeds.

When occupants are present in multiple rooms, signal degradation increases, affecting the classification process. Such a use case is investigated by considering a scenario in which 505 samples are collected from room C for walk/empty cases, when another mobile user is present in room A. In this case, both the occupants walk parallel to the North–South wall. The prediction scores shown in Table XI reveals that in the presence of multiple occupants, the RSSI-based detection scores drop by at least 21.2%, compared with a single-occupant scenario. However, CSI-based detection shows good prediction accuracies and produces comparable scores on all walk patterns. This analysis shows the ability of the proposed model to adapt to diverse walk patterns and the approach can be suitably scaled to develop motion-enabled smart services.

TABLE XIV
MEAN ACCURACY (AS %) ON STATIONARY ACTIVITIES

Classifier	Empty/ Occupied		Empty/ Static		Walk/ Static	
	RSSI	CSI	RSSI	CSI	RSSI	CSI
Random Forest	94.9	**100**	**94.2**	**100**	**99.5**	**100**
Gradient Boosting	93.6	99.1	92.3	98.5	99.4	99
XG Boost	94.6	99.8	93.9	99.6	99.4	99
Hard Voting	94.9	**100**	**94.2**	**100**	**99.5**	**100**
Soft Voting	**95**	**100**	94	**100**	99.4	99.9

G. Static Activities

To examine the performance of the proposed model in detecting room occupancy when the user is static, 690 new WiFi samples were collected from room A and appended to dataset 4. This includes three static activities—lying, standing, and sitting. Three binary classification scenarios were studied for both RSSI and CSI feature sets—*empty versus occupied* (which includes both walking and static activities), *empty versus static*, and *walking versus static* activities. The mean prediction scores for the above-mentioned cases are shown in Table XIV. The results are comparable to those obtained for *empty versus walking*, as indicated in Table III, and hence validates the ability of the proposed model in detecting room occupancy even when the occupant is stationary.

VI. CONCLUSION AND FUTURE SCOPE

In this article, a device-free human motion detection technique using WiFi RSSI and CSI measurements was proposed. Six different datasets collected using commodity IoT devices from two different locations were used for feature extraction and ensemble model training. Using a simple feature set, the proposed model shows a high mean prediction accuracy of up to 99.7% and 97.8% for LoS and NLoS conditions, respectively. The minimal prediction time and memory usage of the trained models show their suitability for real-time, standalone applications such as occupant-driven energy management of buildings. This work also suggests that commercial IoT devices such as laptops/smartphones can be used for opportunistic motion detection with a reasonably good accuracy. At the same time, lightweight and low-cost IoT devices such as ESP32 can enable walk detection with high degree of accuracy through CSI measurements. This technique can be effectively scaled to develop low-cost solutions for a wide variety of occupant-related sensing applications for building energy management, such as activity recognition and is part of our future work.

REFERENCES

[1] (Jan. 2022). *IEA (2019), The Critical Role of Buildings, IEA, Paris*. [Online]. Available: https://www.iea.org/reports/the-critical-role-of-buildings

[2] R. A. Sater and A. B. Hamza, "A federated learning approach to anomaly detection in smart buildings," *ACM Trans. Internet Things*, vol. 2, no. 4, pp. 1–23, Nov. 2021.

[3] K. Han and J. Zhang, "Energy-saving building system integration with a smart and low-cost sensing/control network for sustainable and healthy living environments: Demonstration case study," *Energy Buildings*, vol. 214, May 2020, Art. no. 109861.

[4] D. Gowsikhaa, S. Abirami, and R. Baskaran, "Automated human behavior analysis from surveillance videos: A survey," *Artif. Intell. Rev.*, vol. 42, no. 4, pp. 747–765, Dec. 2014.

[5] T. Yamada et al., "A stretchable carbon nanotube strain sensor for human-motion detection," *Nature Nanotechnol.*, vol. 6, no. 5, pp. 296–301, May 2011.

[6] Q. Pu, J. K.-Y. Ng, and M. Zhou, "Fingerprint-based localization performance analysis: From the perspectives of signal measurement and positioning algorithm," *IEEE Trans. Instrum. Meas.*, vol. 70, pp. 1–15, 2021.

[7] U. Singh, J.-F. Determe, F. Horlin, and P. De Doncker, "Crowd forecasting based on WiFi sensors and LSTM neural networks," *IEEE Trans. Instrum. Meas.*, vol. 69, no. 9, pp. 6121–6131, Jun. 2020.

[8] D. Halperin, W. Hu, A. Sheth, and D. Wetherall, "Tool release: Gathering 802.11 n traces with channel state information," *ACM SIGCOMM Comput. Commun. Rev.*, vol. 41, no. 1, p. 53, Jan. 2011.

[9] Y. Xie. (2016). *Atheros CSI Tool*. [Online]. Available: http://wands.sg/research/wifi/AtherosCSI/

[10] F. Gringoli, M. Schulz, J. Link, and M. Hollick, "Free your CSI: A channel state information extraction platform for modern Wi-Fi chipsets," in *Proc. 13th Int. Workshop Wireless Netw. Testbeds, Exp. Eval. Characterization*, Oct. 2019, pp. 21–28.

[11] S. M. Hernandez and E. Bulut, "Performing WiFi sensing with off-the-shelf smartphones," in *Proc. IEEE Int. Conf. Pervasive Comput. Commun. Workshops (PerCom Workshops)*, Mar. 2020.

[12] S. M. Hernandez and E. Bulut, "Lightweight and standalone IoT based WiFi sensing for active repositioning and mobility," in *Proc. IEEE 21st Int. Symp. A World Wireless, Mobile Multimedia Networks (WoWMoM)*, Aug. 2020, pp. 277–286.

[13] (Jan. 2022). *ESP32-WROOM-32 Datasheet*. [Online]. Available: https://www.espressif.com/sites/default/files/documentation/esp32_datasheet_en.pdf

[14] W. Wang, A. X. Liu, M. Shahzad, K. Ling, and S. Lu, "Device-free human activity recognition using commercial WiFi devices," *IEEE J. Sel. Areas Commun.*, vol. 35, no. 5, pp. 1118–1131, May 2017.

[15] A. Booranawong, N. Jindapetch, and H. Saito, "A system for detection and tracking of human movements using RSSI signals," *IEEE Sensors J.*, vol. 18, no. 6, pp. 2531–2544, Mar. 2018.

[16] A. Booranawong, N. Jindapetch, and H. Saito, "Adaptive filtering methods for RSSI signals in a device-free human detection and tracking system," *IEEE Syst. J.*, vol. 13, no. 3, pp. 2998–3009, Sep. 2019.

[17] S. Depatla, A. Muralidharan, and Y. Mostofi, "Occupancy estimation using only WiFi power measurements," *IEEE J. Sel. Areas Commun.*, vol. 33, no. 7, pp. 1381–1393, Jul. 2015.

[18] K. Qian, C. Wu, Z. Yang, Y. Liu, and Z. Zhou, "PADS: Passive detection of moving targets with dynamic speed using PHY layer information," in *Proc. 20th IEEE Int. Conf. Parallel Distrib. Syst. (ICPADS)*, Dec. 2014, pp. 1–8.

[19] C. Wu, Z. Yang, Z. Zhou, X. Liu, Y. Liu, and J. Cao, "Non-invasive detection of moving and stationary human with WiFi," *IEEE J. Sel. Areas Commun.*, vol. 33, no. 11, pp. 2329–2342, May 2015.

[20] Y. Gu, J. Zhan, Y. Ji, J. Li, F. Ren, and S. Gao, "MoSense: An RF-based motion detection system via off-the-shelf WiFi devices," *IEEE Internet Things J.*, vol. 4, no. 6, pp. 2326–2341, Dec. 2017.

[21] F. Zhang, C. Wu, B. Wang, H.-Q. Lai, Y. Han, and K. J. R. Liu, "WiDetect: Robust motion detection with a statistical electromagnetic model," *Proc. ACM Interact., Mobile, Wearable Ubiquitous Technol.*, vol. 3, no. 3, pp. 1–24, Sep. 2019.

[22] Y. Jin, Z. Tian, M. Zhou, and H. Wang, "Toward a distribution difference-based passive motion detection system using WiFi signals," *IEEE Sensors J.*, vol. 21, no. 21, pp. 24631–24643, Nov. 2021.

[23] Y. Ma, G. Zhou, and S. Wang, "WiFi sensing with channel state information: A survey," *ACM Comput. Surv.*, vol. 52, no. 3, pp. 1–36, Jul. 2019.

[24] H. Abdelnasser, K. Harras, and M. Youssef, "A ubiquitous WiFi-based fine-grained gesture recognition system," *IEEE Trans. Mobile Comput.*, vol. 18, no. 11, pp. 2474–2487, Nov. 2019.

[25] P. Khan, B. S. K. Reddy, A. Pandey, S. Kumar, and M. Youssef, "Differential channel-state-information-based human activity recognition in IoT networks," *IEEE Internet Things J.*, vol. 7, no. 11, pp. 11290–11302, Nov. 2020.

[26] M. A. A. Haseeb and R. Parasuraman, "Wisture: Touch-less hand gesture classification in unmodified smartphones using Wi-Fi signals," *IEEE Sensors J.*, vol. 19, no. 1, pp. 257–267, Jan. 2019.